Orhan Gülcan*

General Electric Aerospace
Gebze / Kocaeli

Kadir Günaydın

General Electric Aerospace
Gebze / Kocaeli

Uğur Şimşek

General Electric Aerospace
Gebze / Kocaeli

Makale Bilgisi:
Araştırma Makalesi
Gönderilme: 2 Ekim 2023
Kabul: 6 Nisan 2024

*Sorumlu Yazar: Orhan Gülcan
E-mail: ogulcan1981@gmail.com

DOI: https://doi.org/10.56193/matim.1370140

A Numerical Investigation About Shrink Line Formation in TPMS Lattice Structures During LPBF Process

Thermal nature of laser powder bed fusion process (LPBF) causes residual stress formation on the part during printing which may cause penetration of some layers towards inside or outside of the nominal geometry called shrink line. Shrink line affects dimensional accuracy and fatigue life of produced parts. The prediction of shrink line formation via numerical methods is important to mitigate the high cost of trial-and-error printing. This study focused on shrink line formation prediction in triply periodic minimum surface (TPMS) lattices produced by LPBF process. The effect of TPMS type, volume fraction, unit cell size, inclination angle of the lattice with respect to build platform, functional grading and material on shrink line formation were investigated. Numerical results revealed that shrink lines were formed only on Primitive lattices and input or control parameters used in this study directly influence the shrink line penetration depth due to different thermally induced stress formation between successive layers.

Keywords: shrink line, laser powder bed fusion, process simulation, TPMS lattices

INTRODUCTION

Triply periodic minimum surface (TPMS) structures are one type of the lattice structures expressed in mathematical equations, having repeating unit cells in three dimensions, and having zero mean curvature of surface [1]. Due to their light weight and enhanced mechanical properties, TPMS structures have been used in different industrial applications [2].

TPMS structures can be produced with some conventional manufacturing methods, however, due to the advancement in additive manufacturing (AM) modalities, they can also be manufactured with AM to reduce cost, lead time, mold or fixture needs [3]. Laser powder bed fusion (LPBF) process is one of the subcategories of AM technologies where laser energy is used to selectively melt metal powder laid on a build platform layer by layer [4].

Since LPBF method is based on layer-by-layer manufacturing in contrast to conventional manufacturing, it enables manufacturing of very complex geometries like TPMS structures [5]. However, during LPBF process, high thermal gradients occurred between successive layers due to the high energy input of laser which causes some of the layers to penetrate towards the outside of the part boundary and form a notch. These notches are called shrink lines [6] and they have negative effects on dimensional accuracy [7] and fatigue life [8] of the printed parts.

It was observed that although there are studies related with shrinkage in LPBF produced parts, there are limited studies in literature that focuses on shrink line formation in LPBF process. It was stated in the literature that powder size distribution, powder density, the number of powder recycling, laser scan speed, laser power, laser spot size, layer thickness, hatch distance, scanning strategy, post processing etc. have some amount of effect of shrinkage and/or part distortion on LPBF produced parts [9-11]. It was shown that laser power increse and laser scan speed decrease [12], layer thickness decrease [13] and preheating the build platform [14] have positive

effects in reduction of shrinkage and part distortion. To the best of authors' knowledge, there are no study so far investigating the shrink line formation in TPMS lattice structures produced by LPBF method. To fill this gap, three different TPMS lattices were investigated in terms of shrink line formation in the present study. Gyroid, Diamond and Primitive structures are three most popular types of TPMS structures whose mathematical expressions are given in equations 1-3 below.

$$Gyroid = \sin\frac{2\pi X}{L_x} * \cos\frac{2\pi Y}{L_y} + \sin\frac{2\pi Y}{L_y} * \cos\frac{2\pi Z}{L_z} + \sin\frac{2\pi Z}{L_z} * \cos\frac{2\pi X}{x} = c \quad (1)$$

$$Diamond = \cos\frac{2\pi X}{L_x} * \cos\frac{2\pi Y}{L_y} * \cos\frac{2\pi Z}{L_z} - \sin\frac{2\pi X}{L_x} * \sin\frac{2\pi Y}{L_y} * \sin\frac{2\pi Z}{L_z} = c \quad (2)$$

$$Primitive = \cos\frac{2\pi X}{L_x} + \cos\frac{2\pi Y}{L_y} + \cos\frac{2\pi Z}{L_z} = c \quad (3)$$

where X, Y, and Z are the number of unit cells and Lx, Ly, and Lz are unit cell dimensions in x, y, and z directions, respectively, c is a constant [15].

It was stated in literature that fracture toughness of Primitive parts are directly affected by volume fraction, unit cell size and number of unit cells [16] which means that there is a direct correlation between these inputs and mechanical properties of TPMS lattices. To show the importance of these factor in terms of shrink line formation, volume fraction, unit cell size, inclination angle of the lattice with respect to build platform, functional grading and material were also selected as input parameters in the present study.

Since LPBF is a costly process, to reduce the cost and build time spent on trial and error printing, numerical methods are widely used to predict the anomalies during and after the build process [17]. Therefore, in this study, thermal and mechanical simulation based numerical methods were used to predict the shrink line formation.

The rest of the paper is organized as follows: in Material and Methods section, specimen design, numerical method, measurement and assessment details were given. In Results section, the result of TPMS type, volume fraction, unit cell size, inclination angle of the lattice with respect to build platform, functional grading and material on shrink line formation were presented and then they were discussed in Discussion section. Finally, summary and main findings were listed in Conclusion section.

MATERIAL AND METHODS

Specimen Design

MsLattice software was used to obtain computer aided (CAD) geometry of TPMS structures. Gyroid, Diamond and Primitive structures were used as TPMS types. Initially 4 mm unit cell size, 6 number of unit cells and 25% volume fraction (the volume percentage of the solid material/feature in TPMS structure) were selected for all TPMS structures (Figure 1). These structures have 0.5 mm wall thickness and 24x24x24 mm outer dimensions. The numerical study on these initial geometries revealed that shrink line were observed on only Primitive structure. Therefore, the rest of the studies were performed on Primitive structures. 35% and 45% volume fractions, 6 mm unit cell size, volumetric functional grading where volume fraction is 25% at the bottom and 45% at the top of the geometry and lastly Inconel 718 and CoCrMo materials were used during numerical investigations. The related design of experiment which contains a total of 11 specimens is shown in Table 1.

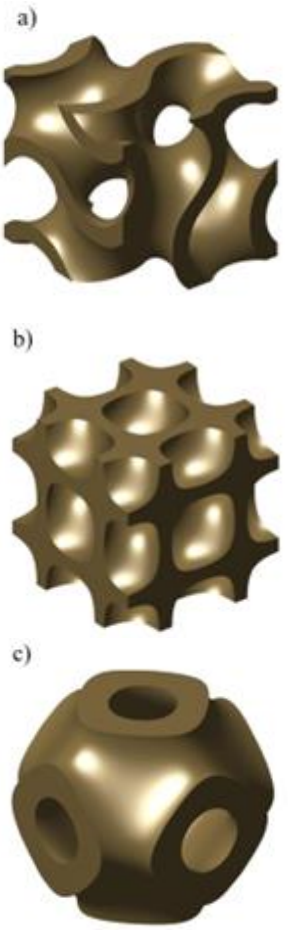

Figure 1. a) Gyroid specimen, b) Diamond specimen, c) Primitive specimen

Numerical Study

For numerical study based on thermomechanical simulations, Simufact Additive 4.1 commercial software was used. For the material data of both CoCrMo and Inconel718, Simufact Material library was used.

The Simufact software uses voxel elements to fully represent the original CAD geometry. The finer voxel elements result in more accurate representation of the geometry but much higher run time. Therefore, a mesh convergence study needs to be performed to obtain the optimum voxel element size for both accuracy and run time. For this purpose, 0.7, 0.6, 0.5, 0.4, 0.3 and 0.2 mm voxel element sizes were used and the results were compared in terms of dimensional deviations. Figure 2 shows the comparison between dimensional deviation and voxel element size. Since dimensional deviation reaches a constant value after a voxel element size of 0.3 mm, this voxel element size value was used in all numerical studies. Each numerical study took nearly 14 hours to complete.

Shrink Line Penetration Depth Measurements

Shrink line penetration depth is important since it affects stress concentration formation and fatigue life reduction. Therefore, this depth is the main performance output of the present study. The deviated geometry based on numerical study was aligned with original CAD geometry in GOM Inspect software and shrink line depts were measured. Shrink line depths were measured on five locations in four side surfaces, therefore, a total of twenty measurements were taken and average of them was used for assessments.

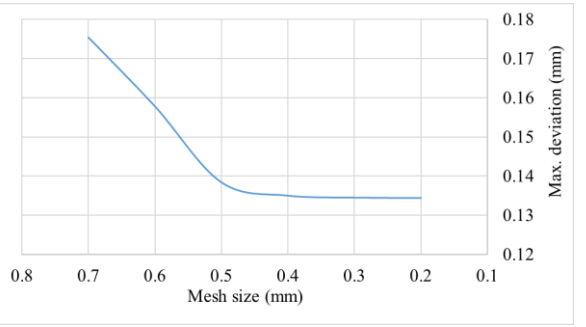

Figure 2. Mesh convergence study

RESULTS

The Effect of TPMS Type on Shrink Line Formation

The displacement of LPBF produced specimens from original CAD data for Gyroid, Diamond and Primitive specimens are shown in Figure 3. It is clear that no distinct shrink line formation was observed on Gyroid and Diamond specimens. However, three shrink lines are clearly visible in Primitive specimen shown with red arrows in Figure 3. Shrink line depths were measured on four surfaces of Primitive specimens and the average values was found as 0.10 mm. There is a shrink line near the top surface of the Primitive specimen, its depth was measured as 0.08 mm, however, it is not clearly visible, therefore, shrink line formation can not be accurately stated in this area.

Table 1. Design of experiment

Specimen No	Lattice type	Volume fraction	Inclination angle of the lattice with respect to build platform (deg.)	Unit cell size (mm)	Number of unit cell	Material
1	Gyroid	0.25	0	6	4	In718
2	Diamond	0.25	0	6	4	In718
3	Primitive	0.25	0	6	4	In718
4	Primitive	0.35	0	6	4	In718
5	Primitive	0.45	0	6	4	In718
6	Primitive	0.25	0	4	6	In718
7	Primitive	0.25-0.45	0	6	4	In718
8	Primitive	0.25	0	6	4	CoCr
9	Primitive	0.25	15	6	4	In718
10	Primitive	0.25	30	6	4	In718
11	Primitive	0.25	45	6	4	In718

The Effect of Volume Fraction on Shrink Line Formation

The displacement of LPBF produced Primitive specimens from original CAD data for different volume fractions are shown in Figure 4. For all the three volume fractions investigated in the present study, a total of four shrink lines were observed in each Primitive specimen. Shrink line depths were measured as 0.10 mm for the bottom three shrink lines and 0.08 mm for the top shrink line. Shrink line depth values for the bottom three shrink lines do not change considerably when volume fraction changes, however, it is clear that when volume fraction increased from 0.25 to 0.35 and then to 0.45, the top shrink line were more clearly visible which indicates a more probable shrink line formation in this region.

The Effect of Unit Cell Size on Shrink Line Formation

The displacement of LPBF produced Primitive specimens from original CAD data for two different unit cell sizes are shown in Figure 5. For Primitive specimen with 6 mm unit cell size and 4 unit cells, a total of four shrink lines were observed and as stated before shrink line depths were measured as 0.10 mm for the bottom three shrink lines and 0.08 mm for the top shrink line. On the other hand, for Primitive specimen with 4 mm unit cell size and 6 unit cells, a total of five shrink lines were observed and shrink line depths were measured as 0.10 mm for the top four shrink lines and 0.07 mm for the bottom shrink line.

The Effect of Functional Grading on Shrink Line Formation

The displacement of LPBF produced Primitive specimens from original CAD data for fixed and variable graded specimens in terms of volume fraction are shown in Figure 6. It is clear that adding functional grading did not change the number of shrink lines when compared with the fixed grading, however, shrink lines depth measurements revealed that bottom and top shrink lines have 0.09 mm depth, and two shrink lines at the middle have 0.10 mm depth in functionally graded specimen contrary to fixed graded specimen in which bottom three shrink lines have 0.10 mm depth and top shrink line has 0.08 mm depth.

The Effect of Inclination Angle on Shrink Line Formation

The displacement of LPBF produced Primitive specimens from original CAD data for different inclination angles with respect to build platform are shown in Figure 7. It is clear that for 0 degree inclination angle, a full smooth shrink lines that pass all the four faces were observed. On the other hand, when inclination angles increased to 30, 45 or 60 degrees, local shrink lines parallel to the build platform (z direction) were observed. The shrink line depths of these local shrink lines are 0.08-0.09 mm. Therefore, it can be stated that tilting the Primitive specimens with respect build platform helps to mitigate shrink lines.

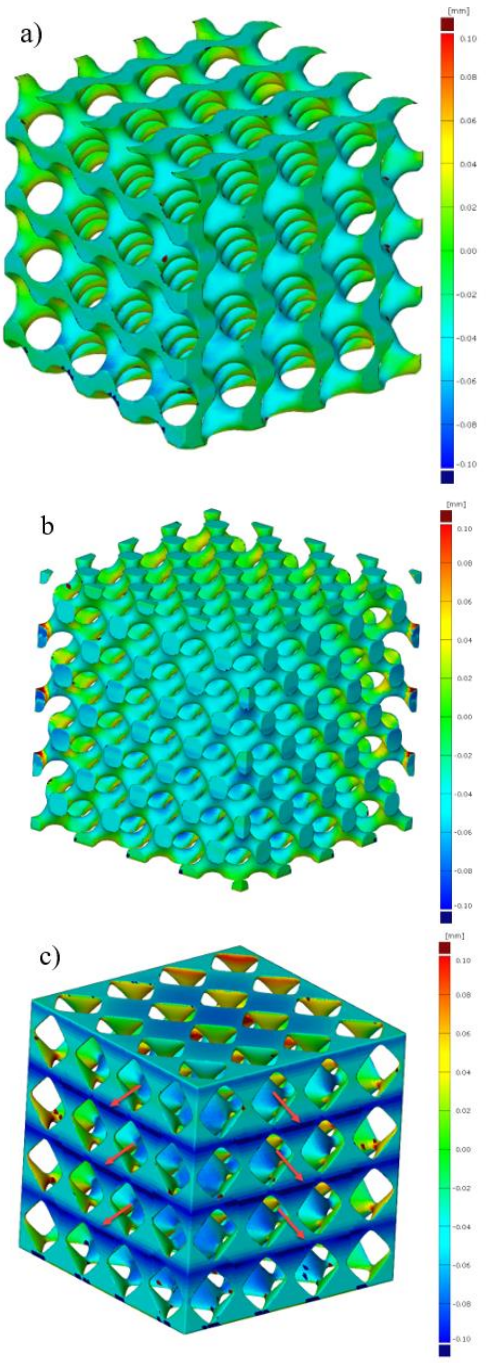

Figure 3. Displacement of LPBF produced specimens from original CAD data for a) Gyroid specimen, b) Diamond specimen, c) Primitive specimen

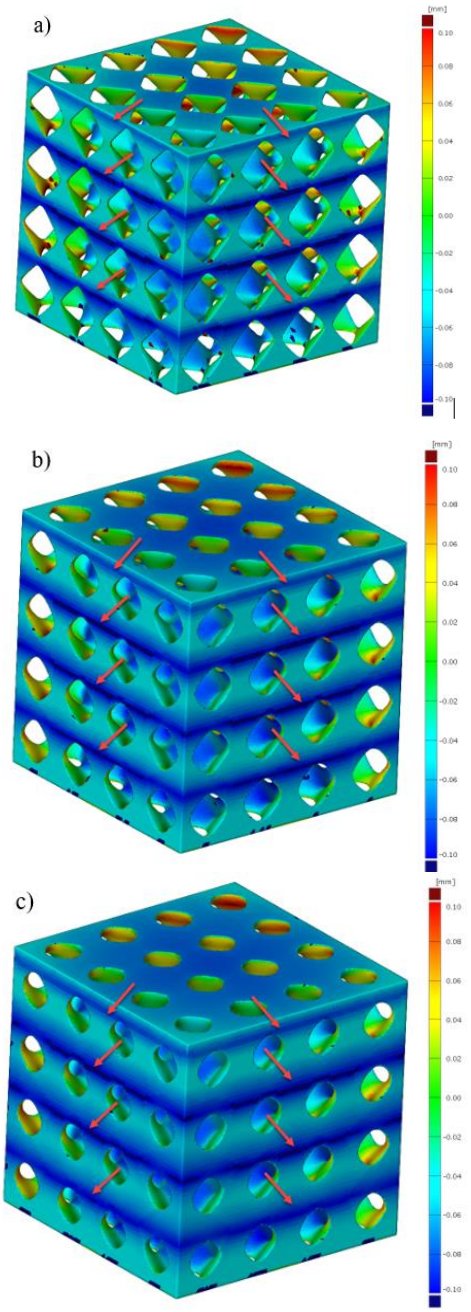

Figure 4. Displacement of LPBF produced Primitive specimens from original CAD data for a) 0.25 volume fraction, b) 0.35 volume fraction, c) 0.45 volume fraction

The Effect of Material on Shrink Line Formation

The displacement of LPBF produced Primitive specimens from original CAD data for Inconel 718 and CoCrMo materials are shown in Figure 8. No distinct difference in terms of shrink line locations were observed between two specimens. However, in terms of shrink line depth 0.01-0.02 mm differences were observed in different locations between two specimens.

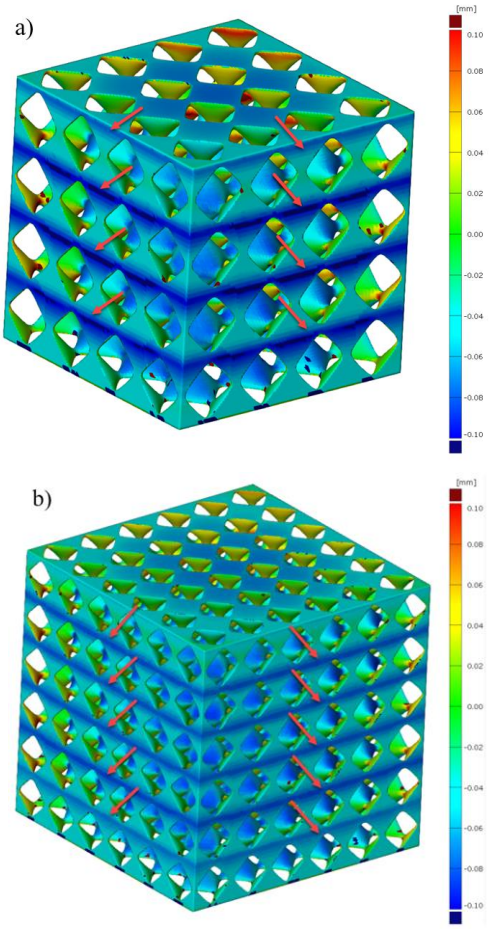

Figure 5. Displacement of LPBF produced Primitive specimens from original CAD data for a) 6 mm unit cell size and 4 unit cells, b) 4 mm unit cell size and 6 unit cells

DISCUSSIONS

LPBF process is a thermal process and due to the local metal powder melting, high thermal gradients occur. These thermal gradients result in local or global warpage of the produced parts. These warpages are more critical especially in cross sectional area changes. If the cross sectional areas between successive layers are somewhat smooth and do not change considerably, then heat dissipation during LPBF process is uniform. On the other hand, if abrupt cross sectional area changes occur between successive layers, then, the heat dissipation becomes variable which causes high tensile forces due to thermal contraction [7].

In the present study, shrink lines were observed only in Primitive specimens. The reason is that Gyroid and Diamond specimens have more uniform cross sectional area changes between successive layers which eliminates shrink line

formation. On the other hand, in Primitive specimens, cross sectional areas increase at the transition of empty pockets to solid walls, and it is clear from Figure 3-8 that shrink lines occurred at these transition areas.

It was observed that volume fraction changes do not change the number of shrink line formation, but it changes the shrink line dept values. The reason is the different thermal input given to each layer. When volume fraction increases, more material is introduced to the specimen and more energy input is needed to scan each layer [18].

Unit cell size directly affected the shrink line formation in terms of number of shrink lines and depth. When unit cell size changed, shrink lines were occurred again at the locations where cross sectional area changes. The depth of shrink lines were different for different unit cell sizes since thermal gradients occurred are different [19, 20]. Similarly, functional grading also affected the shrink line depths due to thermal input and the amount of tensile stress formation [21, 22].

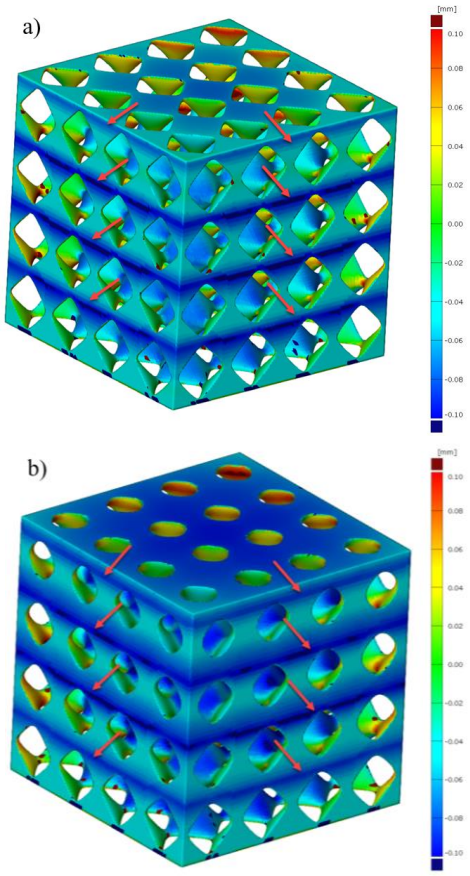

Figure 6. Displacement of LPBF produced Primitive specimens from original CAD data with a) fixed graded volume fraction, b) functionally graded volume fraction.

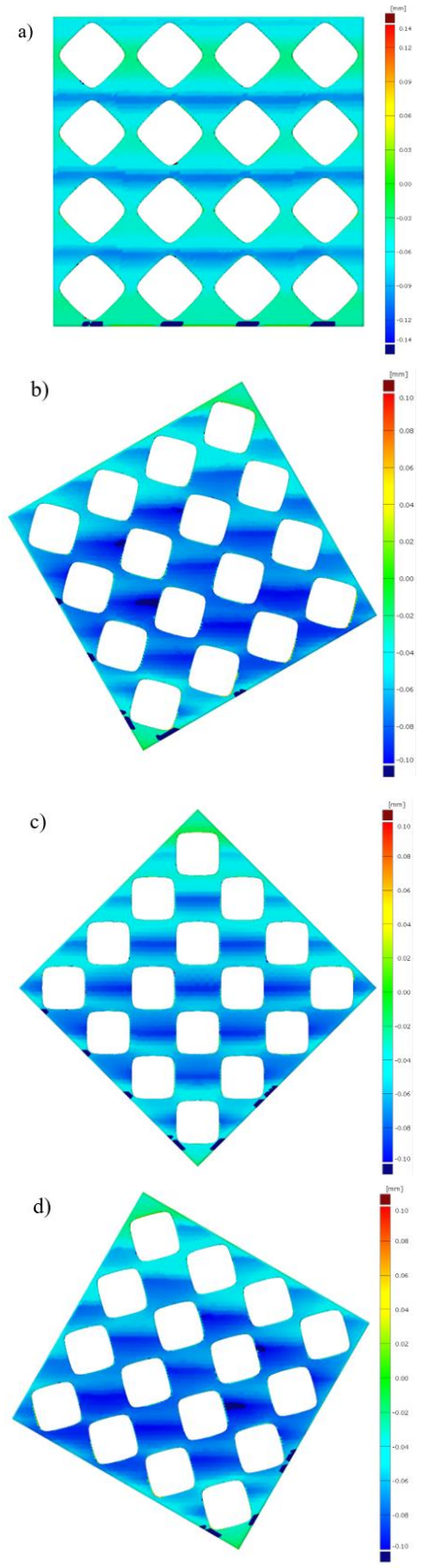

Figure 7. Displacement of LPBF produced Primitive specimens from original CAD data for inclination angle of a) 0 degree, b) 30 degree, c) 45 degree, d) 60 degree

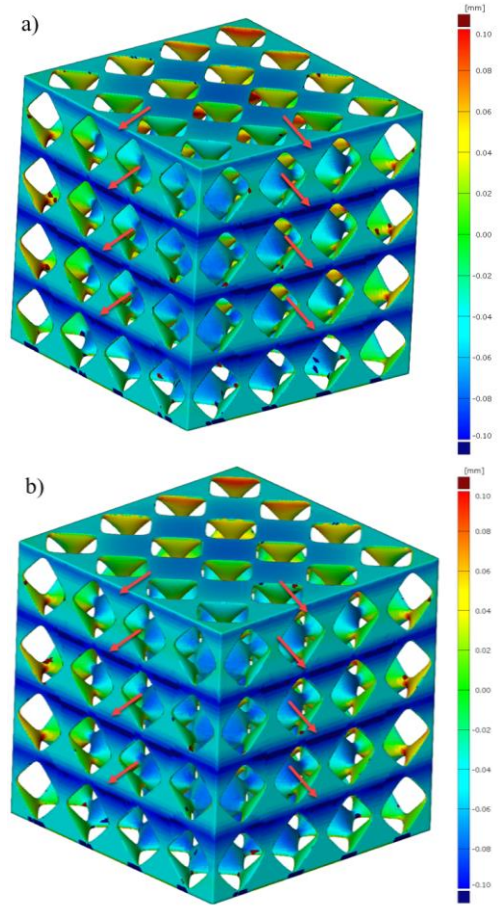

Figure 8. Displacement of LPBF produced Primitive specimens from original CAD data for a) Inconel 718 material, b) CoCrMo material

When inclination of Primitive specimen with respect to build platform changes, cross sectional areas along z direction changes. Therefore, the laser energy given to each layer changes which directly affects the shrink line depth [23].

In LPBF process, different materials can be used to produce end products. These materials have different melting point, therefore the power of laser energy used is different for different materials. Due to different laser power and process parameters, energy input and related thermally induced stresses are different. This is the main reason for different shrink line depths observed in Primitive specimens with Inconel 718 and CoCrMo materials [24].

CONCLUSIONS

Shrink line formation is a very important phenomena in LPBF produced parts which directly affects global dimensional deviation and fatigue life of the part. The prediction of this phenomena before print by using numerical methods is important to decrease the cost and time spent on trial and error printing. In this study, shrink line formation prediction with numerical methods were investigated on three most popular TPMS lattices: Gyroid, Diamond and Primitive. The effect of volume fraction, unit cell size, inclination angle of the lattice with respect to build platform, functional grading and material on shrink line formation were investigated numerically. The main findings can be summarized as follows:

- Due to the sharp cross sectional area changes, shrink line formation was observed only on Primitive specimens.
- Volume fraction, unit cell size, functional grading directly affects shrink line formation and its depth due to the different energy input and thermal induced stress formation.
- Material is one of the most important parameters affecting the shrink line formation due to different laser power and resulting thermal gradients occurred between successive layers.
- Instead of using 0 degree inclination, 30, 45 or 60 degree inclination of lattice structure with respect to build platform can be used to mitigate shrink line formation.

The present study focused on only numerical investigation of shrink line formation. Future studies will focus on experimental testing and verification.

LAZER TOZ YATAĞI FÜZYON PROSESİ SIRASINDA, TPMS KAFES YAPILARINDA OLUŞAN BÜZÜLME ÇİZGİLERİNİN SAYISAL İNCELENMESİ

Lazer toz yatağı füzyon işleminin (LTYF) termal doğası, üretim sırasında parça üzerinde artık gerilim oluşumuna neden olur ve bu da bazı katmanların büzülme çizgisi adı verilen nominal geometrinin içine veya dışına nüfuz etmesine neden olabilir. Büzülme çizgisi, üretilen parçaların boyutsal doğruluğunu ve yorulma ömrünü etkiler. Büzülme çizgisi oluşumunun sayısal yöntemlerle tahmin edilmesi, deneme yanılma üretiminin yüksek maliyetini azaltmak için önemlidir. Bu çalışma, LTYF yöntemi ile üretilen üçlü periyodik minimum yüzey (TPMS) kafeslerinde büzülme çizgisi oluşumunun tahmin edilmesine odaklanmıştır. TPMS tipinin, hacim oranının, birim hücre boyutunun, kafesin üretim platformuna göre eğim açısının, fonksiyonel derecelendirmenin ve malzemenin büzülme çizgisi oluşumuna etkisi araştırılmıştır. Sayısal sonuçlar, büzülme çizgilerinin yalnızca Primitif kafeslerde oluştuğunu ve bu çalışmada kullanılan kontrol parametrelerinin, ardışık katmanlar arasındaki, ısı kaynaklı gerilim oluşumu nedeniyle büzülme çizgisi penetrasyon derinliğini doğrudan etkilediğini ortaya çıkardı.

Anahtar Kelimeler: Büzülme çizgisi, lazer toz yatağı füzyon yöntemi, proses simülasyonu, TPMS kafes yapısı

REFERENCES

1. Pan, C., Han, Y. and Lu, J., Design and optimization of lattice structures: A review, Appl. Sci., 10 (2020) 6374. https://doi.org/10.3390/app10186374.
2. Yuan, Li, Ding, S. and Wen, C., Additive manufacturing technology for porous metal implant applications and triple minimal surface structures: A review, Bioact. Mater., 4 (2019) 56-70. https://doi.org/10.1016/j.bioactmat.2018.12.003.
3. Sokollu, B., Gulcan, O. and Konukseven, E. I., Mechanical properties comparison of strut-based and triply periodic minimal surface lattice structures produced by electron beam melting, Addit. Manuf., 60 (2022) A, 103199. https://doi.org/10.1016/j.addma.2022.103199.
4. Sefene, E. M., State-of-the-art of selective laser melting process: A comprehensive review, J. Manuf. Syst., 63 (2022) 250-274. https://doi.org/10.1016/j.jmsy.2022.04.002.
5. Gong, G., Ye, J., Chi, Y., Zhao, Z., Wang, Z., Xia, G., Du, X., Tian, H., Yu, H. and Chen, C., Research status of laser additive manufacturing for metal: a review, J. Mater. Res. Technol., 15 (2021) 855-884. https://doi.org/10.1016/j.jmrt.2021.08.050.
6. Adam, G. A. O. and Zimmer, D., Design for Additive Manufacturing—Element transitions and aggregated structures, CIRP J. Manuf. Sci. Technol., 7 (2014) 1, 20-28. https://doi.org/10.1016/j.cirpj.2013.10.001.
7. Goetz, D., Wolf, D., Lehmann, M. and Zaeh. M. F., A novel approach for the quantitative characterization of shrink lines in the Powder Bed Fusion of metals using a laser beam, Procedia CIRP, 111 (2022) 832-837. https://doi.org/10.1016/j.procir.2022.08.093.
8. Richardsen, S., Crawford and G., Gockel, J., Effect of a build pause on the fatigue behavior of laser powder bed fusion 316L stainless steel with as-build surfaces, Eng. Fail. Anal., 153 (2023) 107590. https://doi.org/10.1016/j.engfailanal.2023.107590.
9. Sanchez, S., Smith, P., Xu, Z., Gaspard, G., Hyde, C. J., Wits, W. W., Ashcroft, I. A., Chen, H. and Clare, A. T, Powder Bed Fusion of nickel-based superalloys: A review, Int. J. Mach. Tools Manuf. 165 (2021) 103729. https://doi.org/10.1016/j.ijmachtools.2021.103729.
10. Dowling, L., Kennedy, J., O'Shaughnessy, S. and Trimble, D, A review of critical repeatability and reproducibility issues in powder bed fusion, Materi Des. 186 (2020) 108346. https://doi.org/10.1016/j.matdes.2019.108346.
11. Avrampos, P. and Vosniakos, G. -C., A review of powder deposition in additive manufacturing by powder bed fusion, J. Manuf. Proces. 74 (2022) 332-352. https://doi.org/10.1016/j.jmapro.2021.12.021.
12. Levkulich, N. C., Semiatin, S. L., Gockel, J. E., Middendorf, J. R., DeWald, A. T. and Klingbeil, N. W., The effect of process parameters on residual stress evolution and distortion in the laser powder bed fusion of Ti-6Al-4V, Addit. Manuf. 28 (2019) 475-484. https://doi.org/10.1016/j.addma.2019.05.015.
13. Mukherjee, T., Zhang, W. and DebRoy, T., An improved prediction of residual stresses and distortion in additive manufacturing, Comput. Mater. Sci. 126 (2017) 360-372. https://doi.org/10.1016/j.commatsci.2016.10.003
14. Buchbinder, D., Meiners, W., Pirch, N. and Wissnebach, K., Investigation on reducing distortion by preheating during manufacture of aluminum components using selective laser melting, J. Laser Appl. 26 (2014) 012004. https://doi.org/10.2351/1.4828755.
15. Zheng, N., Zhai, X. and Chen, F., Topology optimization of self-supporting porous structures based on triply periodic minimal surfaces, Comput. Aided Des., 161 (2023) 103542. https://doi.org/10.1016/j.cad.2023.103542.
16. Almomani, A. and Mourad, A. I., The fracture toughness of Schwarz Primitive triply periodic minimal surface lattice, Theor. App. Fract. Mech., 125 (2023) 103924. https://doi.org/10.1016/j.tafmec.2023.103924.
17. Denlinger, E. R., Gouge, M., Irwin, J. and Michaleris, P., Thermomechanical model development and in situ experimental validation of the Laser Powder-Bed Fusion process, Addit. Manuf., 16 (2017) 73-80. https://doi.org/10.1016/j.addma.2017.05.001.
18. Yan, C., Hao, L., Hussein, A., Bubb, S. L., Young, P. and Raymont, D., Evaluation of light-weight AlSi10Mg periodic cellular lattice structures fabricated via direct metal laser sintering, J. Mater. Process. Technol., 214 (2014) 856-864. https://doi.org/10.1016/j.jmatprotec.2013.12.004.
19. Yan, C., Hao, L., Hussein, A., Young, P., Huang, J. and Zhu, W., Microstructure and mechanical properties of aluminum alloy cellular lattice structures manufactured by direct metal laser sintering, Mater. Sci. Eng. A, 628 (2015) 238-246. https://doi.org/10.1016/j.msea.2015.01.063.
20. Mishra, A. K., Chavan, H. and Kumar, A., Effect of cell size and wall thickness on the compression performance of triply periodic minimal surface based AlSi10Mg lattice

structures, Thin-Walled Struct., 193 (2023) 111214. https://doi.org/10.1016/j.tws.2023.111214.
21. Yang, L., Mertens, R., Ferrucci, M., Yan, C., Shi, Y. and Yang, Y., Continuous graded Gyroid cellular structures fabricated by selective laser melting: Design, manufacturing and mechanical properties, Mater. Des., 162 (2019) 394-404. https://doi.org/10.1016/j.matdes.2018.12.007.
22. Qiu, N., Zhang, J., Li, C., Shen, Y. and Fang, J., Mechanical properties of three-dimensional functionally graded triply periodic minimum surface structures, Int. J. Mech. Sci., 246 (2023) 108118. https://doi.org/10.1016/j.ijmecsci.2023.108118.
23. Weißmann, V., Drescher, P., Bader, R., Seitz, H., Hansmann, H. and Laufer, N., Comparison of single Ti6Al4V struts made using selective laser melting and electron beam melting subject to part orientation, Metals, 7 (2017) 3, 91. https://doi.org/10.3390/met7030091.
Sing, S. L., Wiria, F. E. and Yeong, W. Y., Selective laser melting of lattice structures: A statistical approach to manufacturability and mechanical behavior, Robot. Comput. Integr. Manuf., 49 (2018) 170-180. https://doi.org/10.1016/j.rcim.2017.06.006.